

Signatures of Fractional Quantum Hall States in Topological Insulators

Dong-Xia Qu^{1*}, Y. S. Hor², R. J. Cava², and N. P. Ong¹

*Department of Physics¹ and Department of Chemistry²,
Princeton University, New Jersey 08544, USA.*

(Dated: February 11, 2022)

The fractional quantum Hall (FQH) state is a topological state of matter resulting from the many-body effect of interacting electrons and is of vast interest in fundamental physics. Recent theoretical studies suggest that the FQH effect might be observable in topological insulators, which can host a single Dirac valley with no spin degeneracy. However, due to the dominant bulk conduction it is difficult to probe the strong correlation effect in topological insulators from resistivity measurements. Here we report the discovery of FQH states in Bi₂Te₃ from thermopower measurements. The surface thermopower is ten times greater than that of bulk, which makes possible the observation of fractional-filled Landau levels in surface states. Hence, thermopower provides a powerful tool to investigate correlated Dirac fermions in topological insulators.

PACS numbers: *All correspondence should be addressed to D. Qu (dqu@princeton.edu).

Topological insulators (TIs) are a new class of quantum states of matter with topologically protected conducting surface states, arising from the topology of the bulk electronic band structure [1–8]. There are two distinguishing features of topological surface states. One is the existence of an odd number of Dirac cones on each surface, and the other is the helical spin arrangement [9–17]. Theoretically, the relativistic nature of Dirac fermions is believed to significantly modify the electron-electron interactions, with the possibility to produce more robust ground states at the $n = 1$ Landau level (LL) in TIs than in conventional two-dimensional electron systems [18–21]. The unique spin texture and the coexistence of non-insulating bulk states also raise the intriguing question of whether TIs may host exotic FQH states owing to the non-trivial Berry's phase [22], huge Zeeman energy [23], and the screening effect from bulk carriers [21]. The potential realization of more stable non-Abelian FQH states in TIs is of practical interest for topological quantum computing. However, up to date no experiments have unambiguously detected the FQH states in TIs because the introduction of dopants tremendously reduces the surface mobility and the surface conduction is always obscured by the residual bulk contribution.

To explore the existence of FQH states in TIs, we have performed thermoelectric measurements on the Bi₂Te₃ crystals. The surface mobility of these crystals is in the range of 8,600–14,000 cm²V⁻¹s⁻¹, comparable to the Hall mobility (30,000 cm²V⁻¹s⁻¹) of high quality graphene where the FQH effect has been recently discovered [24]. We first examined the dependence of thermopower S_{xx} on temperature T in both metallic and nonmetallic samples (Fig. 1, insets). Though S_{xx} shows a low- T peak in all these samples, the peak of the non-metallic samples Q1 and Q2 is significantly stronger than that of the metallic sample M1. These observed peaks indicate the occurrence of phonon-drag effect that is expected to appear at ~ 29 K in high purity Bi₂Te₃ crystals [25]. It has been demonstrated that the phonon-drag thermopower from a two-dimensional (2D) conducting

layer on a three-dimensional (3D) crystal can display giant quantum oscillations due to the phonon intra- and inter-LL scattering in the presence of a strong magnetic field. In such a 3D system, surface electrons are dragged by non-equilibrium 3D phonons of the whole specimen, while in a purely 2D system such as graphene, electrons of a wavevector k can only interact with 2D phonons of a wavevector $q \leq 2k$. In addition, the bulk thermopower is considerably suppressed due to the existence of two types of bulk carriers with opposite signs [14]. Therefore, we expect that the magneto-thermopower of surface states is orders of magnitude larger than that of bulk in the high field limit. The thermopower measurement thus provides a powerful tool to elucidate the nature of the topological surface state that is difficult to be probed by the conductance measurement.

Figure 1, A and B, show the thermopower response $-S_{xx}$ versus the inverse magnetic field $1/H$ in samples Q1 and Q2, respectively. Large Landau level oscillations begin to emerge at $1/H < 0.12$ T⁻¹. As the chemical potential μ lies between adjacent LLs, a sharp dip appears in the $-S_{xx}$ versus H ($S_{xx} < 0$ for electron carriers and the dips in $-S_{xx}$ signal the minimum surface contribution). In terms of the carrier density n_e on one surface, the dips occur at the fields B_ν given by

$$B_\nu = \frac{n_e \phi_0}{(\nu - \gamma)} \quad (1)$$

where $\phi_0 = h/e$ is the magnetic flux quanta, h Planck's constant, e the charge of electron, and γ the filling factor shift. A shift with $\gamma = 0$ corresponds to a conventional spectrum, whereas a deviation from the zero-shift with $\gamma = 1/2$ implies a Dirac spectrum. The $1/2$ arises from the $n = 0$ Landau level at the Dirac point. We label the filling factors as ν^s , where $s = \pm$ indexes the top and bottom surface states.

We have identified two sets of Landau level oscillations for both samples (Fig. 1). The Landau level splitting occurs because there is a weak Fermi energy (E_F) gradient in as-grown Bi₂Te₃. By cleaving the crystal into bulk

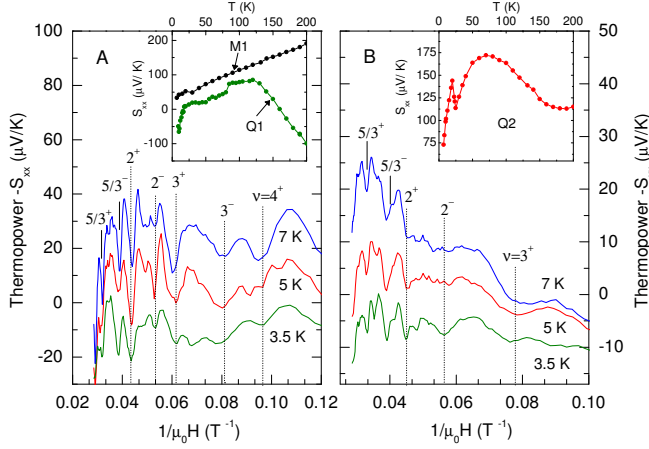


FIG. 1: The thermopower response versus $1/H$ in (A) sample Q1 and (B) sample Q2 at temperatures $T = 3.5, 5$, and 7 K. The insets show the T dependence of the thermopower profiles in samples Q1 and M1 (A) and in sample Q2 (B). The dotted lines mark the integer-filling factors of the top (+) and bottom (-) surface states. The short lines indicate the positions of $B_v = n_e \phi_0 / (\nu - \gamma)$, where n_e is obtained from the slope of the SdH oscillations and γ is determined from the index plot. $n_e = 9.30$ (7.60) $\times 10^{11}$ and 7.37 (5.92) $\times 10^{11}$ cm^{-2} for the top (bottom) surface states in Q1 and Q2, respectively. $\gamma \approx 0.5$ and 0.67 in Q1 and Q2, respectively.

samples with a thickness $t = 20 \sim 100$ μm , we obtain slightly different E_F or equivalently different carrier densities on two surfaces. For $1/H > 0.04$ T^{-1} , the integer index fields B_{ν^s} appear as sharp minima in $-S_{xx}$. Their $B_{\nu^s}^{-1}$ positions are close to those minima resolved in the conductivity tensor. For $1/H < 0.04$ T^{-1} , we observed sharp, reproducible dips at the fields B_{ν^s} (solid lines) with the fractional-filling factor $\nu^s = 5/3^\pm$. As T decreases from 7 to 3.5 K, these features become sharper but their amplitudes become smaller.

We then illustrate the fine structure of the high-field oscillations in Fig. 2, A and B. In addition to the dips at $\nu^s = 5/3^\pm$, a valley-like structure at $\nu^s = 9/5^\pm$ is discernable in Q1, and the dip at $\nu^s = 9/5^+$ becomes prominent in Q2 as the temperature decreases. In the plots of $B_{\nu^s}^{-1}$ versus ν (Fig. 2, C and D), all the fractional Landau fillings lie on a straight line with the integer ones, observed in both the thermopower and resistivity measurements. The slopes yield the carrier density $n_e = 9.30$ (7.60) $\times 10^{11}$ and 7.37 (5.92) $\times 10^{11}$ cm^{-2} for the top (bottom) surface states in samples Q1 and Q2, respectively. The linear fit to the data intercepts the ν axis at 0.5 in Q1 and 0.67 in Q2, consistent with a Dirac dispersion. Hence, the 2D Dirac states give rise to the Landau level indexing shown in Fig. 1.

To examine the oscillating profiles of the sub-integer dips, we plot the $-S_{xx}$ versus the filling factor estimated as $\nu = n_e \phi_0 B^{-1} + \gamma$ (Fig. 3, A and B). The $-S_{xx}(\nu)$ traces obtained at different surface carrier densities are almost overlapped, and their minima are all located around $\nu = 1.67 \pm 0.02$ (traces are displaced for

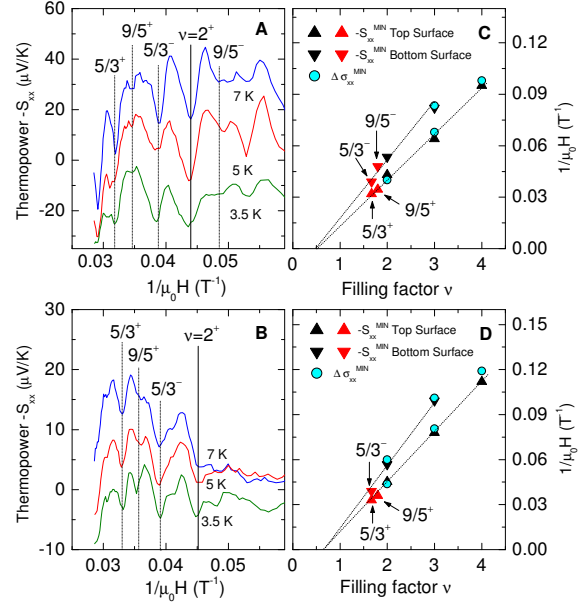


FIG. 2: The high-field thermopower response versus $1/H$ in (A) sample Q1 and (B) sample Q2. Identified dips correspond to the fractional-filling factors illustrated as the vertical dashed lines. Note that the dips at $\nu = 5/3^+$ and $5/3^-$ are much stronger than those at $\nu = 9/5^+$ and $9/5^-$. The $1/H$ positions of the $-S_{xx}$ and $\Delta\sigma_{xx}$ minima versus the filling factor ν in (C) sample Q1 and (D) sample Q2. The black and red triangles represent the integer- and fractional fillings, respectively.

clarity). Both features suggest that the observed high-field dips are associated with the fractional quantum Hall states with $1 < \nu < 2$.

We next extracted the surface thermopower S_{xx}^s from the observed thermopower response. The measured thermopower tensor S_{ij} can be expressed as the sum,

$$S_{ij} = \sum_{k=x,y} \rho_{ik} (\alpha_{kj}^b + \frac{\alpha_{kj}^s}{t}) \quad (2)$$

where ρ_{ij} is the total resistivity tensor, $\alpha_{ij}^l = \sum_{k=x,y} \sigma_{ik}^l S_{kj}^l$ with $l = b$ or s , the bulk or surface thermoelectric conductivity tensor, and σ_{ij}^l the bulk or surface conductivity tensor. Since $\rho_{xx} \gg \rho_{yx}$, $\sigma_{xx}^b \gg \sigma_{xy}^b$, $\sigma_{xx}^s \gg \sigma_{xy}^s$, and $\sigma_{xx} \gg \sigma_{xy}$ for nonmetallic Bi_2Te_3 in the high-field regime, S_{xx} can be approximated as

$$S_{xx} = S_{xx}^b + \frac{1}{t} \rho_{xx} G_{xx}^s S_{xx}^s \quad (3)$$

where S_{xx}^b is the bulk thermopower and G_{xx}^s the surface conductance. The bulk thermopower is only gives rise to a featureless background. The $\rho_{xx} G_{xx}^s / t$ term can be obtained from the resistivity measurements (Fig. S3 and S4). We find that the maximum magnitude of $\rho_{xx} G_{xx}^s / t \approx 0.027$ and 0.01 in Q1 and Q2, respectively. From Eq. (3), we can extract the $-S_{xx}^s$ versus H in Q1 and Q2 (Fig. 3, C and D, red curves). The peak magnitude of $-S_{xx}^s$ is in the range of 0.5 – 2.0 mV K^{-1} , which is

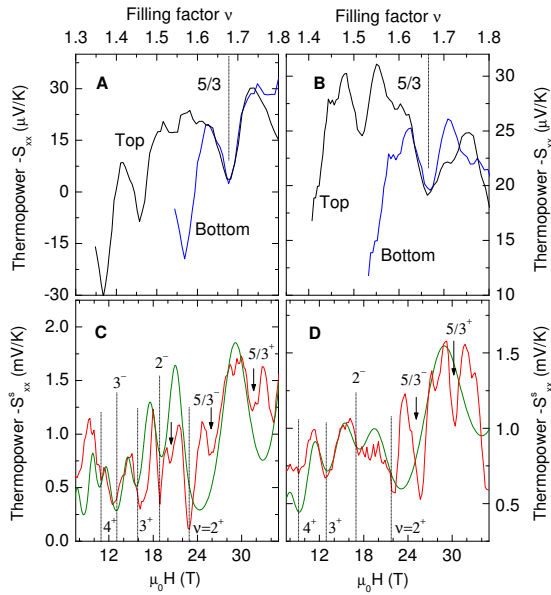


FIG. 3: (A) $-S_{xx}$ as a function of the filling factor $\nu = n_e \phi_0 B^{-1} + \gamma$ in sample Q1 at 7 K. (B) $-S_{xx}$ versus ν in sample Q2 at 7 K. The surface thermopower $-S_{xx}^s$ obtained by removing a smooth background contributed from S_{xx}^b in sample Q1 (C) and sample Q2 (D) at 5 K. The green curve is the fit to $-S_{xx}^s$ (SOM, S3). The H positions at the integer-filling factors are marked by dotted lines. The fractional dips resolved at $\nu > 2^-$ are indicated by arrows.

more than ten times higher than that of the bulk $\sim 30 \mu\text{V K}^{-1}$ at 5 K. Unlike conventional 2D systems where the thermopower magnitude roughly displays a linear field dependence [26], the surface thermopower at higher order Landau levels such as $n = 4$ is comparable or even greater than that of lower Landau levels ($n = 3$) in both Q1 and Q2.

The giant oscillating magnitude and the specific field profile of the surface thermopower can be understood within the scenario of the 2D Dirac electron and 3D phonon interaction. As a consequence of the relativistic dispersion of topological surface states, the wave function Ψ_n of a Dirac electron in the n th Landau level is the superposition of the n th and $(n - 1)$ th Landau level wave functions of a non-relativistic electron. The unique Landau quantization of surface states leads to a particular thermopower profile, different from an ordinary 2D system. Because the mixture nature of the wave function modifies the electron-phonon interaction within and between LLs, which determines the thermopower oscillation at each Landau level.

Using a general model given in [27] and the wave function for topological surface states [28], we numerically simulated the thermopower induced by the integer Landau quantization in Q1 and Q2 (Fig. 3, C and D, green curves). The simulation yields the phonon mean free path $\Lambda_{qs} \sim 81$ and $179 \mu\text{m}$ in Q1 and Q2, respectively. We deduce the average Landau level broadening width $\Gamma = 3.5$ and 7 meV for Q1 and Q2, respectively. They are 2 \sim 3 times smaller than the value of the GaAs sys-

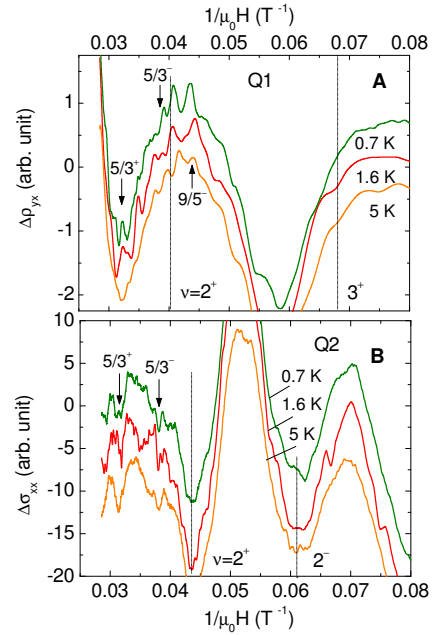


FIG. 4: (A) The inverse field dependence of $\Delta\rho_{yx}$ in sample Q1 at $T = 0.7, 1.6$, and 5 K . (B) $\Delta\sigma_{xx}$ versus $1/H$ in sample Q2 at selected temperatures. The black dotted lines mark the value of the integer-filling factor. The black arrows indicate the emerging fractional-filling states.

tem with a similar mobility. It may result from the protected nature of topological surface states. Both the field profile and the magnitude of integer Landau oscillations so calculated agree well with the experimental results. Therefore, we are convinced that the observed quantum oscillations indeed arise from the Dirac fermion and 3D phonon interaction.

In addition to the integer quantization, the fractional-filling states also display resonant amplitudes on the order of 0.5 to 1.0 mV K^{-1} (Fig. 3, C and D, black arrows). We can preclude the possibility that these oscillations might come from a 2D hole accumulation layer due to the band bending. If the sharp resonance at $H = 26 \text{ T}$ was ascribed to a 2D p -type band, the band would have had a mobility μ_h comparable to $8,000 \text{ cm}^2 \text{V}^{-1} \text{s}^{-1}$ and a hole density $n_h = 7.6 \times 10^{11} \text{ cm}^{-2}$ ($n_h = B\nu/\phi_0$, $\nu = 1$). In this way, the Hall conductance from the high-mobility p -type band would completely wipe out the Hall conductance from the n -type surface band, making impossible the observation of the surface Hall anomaly [14].

To demonstrate more evidences of the FQH states, we carried out resistivity measurements in Q1 and Q2 at a magnetic field up to 35 T . In sample Q1, extra peaks are present in $\Delta\rho_{yx}$ at $\nu^s = 5/3^\pm$ and $9/5^-$, which also suggest the emerging FQH states (Fig. 4A, black arrows). As T increases from 0.7 to 5 K , their oscillating amplitudes decrease rapidly. In sample Q2, two sub-integer dips can be clearly resolved in $\Delta\sigma_{xx}$ with the minima close to $\nu^s = 5/3^\pm$ (Fig. 4B, black arrows). By comparing the fractional-filling states observed in the resistivity and thermopower measurements, we find that the $5/3$ state is more robust than the $9/5$ state, as expected from

the theoretical predictions [19, 20].

The lower bound of the gap energy of the 5/3 state ($\Delta_{5/3}$) can be estimated from the T dependence of the resistivity measurements. In Fig. 4A, we observed that the 5/3⁺ state almost vanishes at 5 K, indicating $\Delta_{5/3} \sim 5$ K. The observed $\Delta_{5/3}$ is more than an order of magnitude larger than the corresponding gap ($\Delta_{8/3}$) in the GaAs system with a much higher mobility [29]. This is not surprising because the $n = 1$ Landau level in the topological surface states is a mixture of the $n = 0$ and 1 LLs in non-relativistic systems. It makes the FQH states in the $n=1$ Landau level in the Dirac system more robust than those in the GaAs system [18–20, 30–32].

We also note that the gap value of $\Delta_{5/3}$ is comparable to the corresponding gap in graphene with a higher mobility [24]. This property implies that the 5/3 state is more stable in TIs. Compared with graphene, the surface states in Bi₂Te₃ has only one Dirac valley with no spin degeneracy, analogous to a completely four-fold degeneracy lifted graphene system where the FQH states do not mix between spin- and valley-bands. Indeed, the

5/3 gap is $\sim 0.16e^2/\epsilon l_B$ in Coulomb energy units (the dielectric constant ϵ is 85 in Bi₂Te₃ and $l_B = (\hbar/eB)^{1/2}$ is the magnetic length), which is in good agreement with the theoretical calculation, $\Delta_{5/3} \approx 0.2e^2/\epsilon l_B$, in the fully spin- and valley-polarized graphene system [19]. Moreover, the helical spin texture of topological surface states and the presence of conductive bulk states may lead to enhanced effective Coulomb interactions, rendering the FQH states even more robust in TIs.

By performing thermopower measurements, we have resolved fractional Landau quantization of surface states at $\nu = 5/3$ and $9/5$. The observed gap energy at the 5/3 state is ten times larger than that of the non-relativistic electron systems. The demonstration of the FQH states in the topological surface bands opens the door to future studies of fractional quantum Hall effect physics in the topological insulator, which is expected to display strong correlation effects between chiral Dirac fermions.

The authors would like to thank F. D. Haldane and C.-X. Liu for helpful discussion.

-
- [1] C. L. Kane and E. J. Mele, Phys. Rev. Lett. **95**, 146802 (2005).
 - [2] B. A. Bernevig and S.-C. Zhang, Phys. Rev. Lett. **96**, 106802 (2006).
 - [3] B. A. Bernevig, T. L. Hughes, and S.-C. Zhang, Science **314**, 1757 (2006).
 - [4] M. König, S. Wiedmann, C. Röhne, A. Roth, H. Buhmann, L. W. Molenkamp, X.-L. Qi, and S.-C. Zhang, Science **318**, 766 (2007).
 - [5] J. E. Moore and L. Balents, Phys. Rev. B **75**, 121306 (R) (2007).
 - [6] L. Fu and C. L. Kane, Phys. Rev. B **76**, 045302 (2007).
 - [7] L. Fu, C. L. Kane, and E. J. Mele, Phys. Rev. Lett. **98**, 106803 (2007).
 - [8] H. Zhang, C.-X. Liu, X.-L. Qi, X. Dai, Z. Fang, and S.-C. Zhang, Nat. Phys. **5**, 438 (2009).
 - [9] D. Hsieh, D. Qian, L. Wray, Y. Xia, Y. S. Hor, R. J. Cava, and M. Z. Hasan, Nature **452**, 970 (2008).
 - [10] P. Roushan, J. Seo, C. V. Parker, Y. S. Hor, D. Hsieh, D. Qian, A. Richardella, M. Z. Hasan, R. J. Cava, and A. Yazdani, Nature **460**, 1106 (2009).
 - [11] D. Hsieh, Y. Xia, L. Wray, D. Qian, A. Pal, J. H. Dil, J. Osterwalder, F. Meier, G. Bihlmayer, C. L. Kane, et al., Science **323**, 919 (2009).
 - [12] Y. Xia, L. Wray, D. Qian, D. Hsieh, A. Pal, H. Lin, A. Bansil, D. Grauer, Y. Hor, R. Cava, et al., Nat. Phys. **5**, 398 (2009).
 - [13] Y. L. Chen, J. G. Analytis, J. H. Chu, Z. K. Liu, S.-K. Mo, X. L. Qi, H. J. Zhang, D. H. Lu, X. Dai, Z. Fang, et al., Science **325**, 178 (2009).
 - [14] D.-X. Qu, Y. S. Hor, J. Xiong, R. J. Cava, and N. P. Ong, Science **329**, 821 (2010).
 - [15] P. Cheng, C. Song, T. Zhang, Y. Zhang, Y. Wang, J.-F. Jia, J. Wang, Y. Wang, B.-F. Zhu, X. Chen, et al., Phys. Rev. Lett. **105**, 076801 (2010).
 - [16] T. Hanaguri, K. Igarashi, M. Kawamura, H. Takagi, and T. Sasagawa, Phys. Rev. B **82**, 081305 (2010).
 - [17] J. G. Analytis, R. D. McDonald, S. C. Riggs, J.-H. Chu, G. S. Boebinger, and I. R. Fisher, Nature Phys. **6**, 960 (2010).
 - [18] K. Yang, S. D. Sarma, and A. H. MacDonald, Phys. Rev. B **74**, 075423 (2006).
 - [19] V. M. Apalkov and T. Chakraborty, Phys. Rev. Lett. **97**, 126801 (2006).
 - [20] C. Toke, P. E. Lammert, V. H. Crespi, and J. K. Jain, Phys. Rev. B **74**, 235417 (2006).
 - [21] A. M. DaSilva, Solid State Communications **10**, 1016 (2011).
 - [22] S.-Y. Xu, Y. Xia, L. A. Wray, S. Jia, F. Meier, J. H. Dil, J. Osterwalder, B. Slomski, A. Bansil, H. Lin, et al., Science **332**, 560 (2011).
 - [23] B. I. Halperin, P. A. Lee, and N. Read, Phys. Rev. B **47**, 7312 (1993).
 - [24] C. R. Dean, A. F. Young, P. C.-Zimansky, L. Wang, H. Ren, K. Watanabe, T. Taniguchi, P. Kim, J. Hone, and K. L. Shepard, Nature Phys. **10**, 1038 (2011).
 - [25] C. Kittel, *Introduction to Solid State Physics* (John Wiley & Sons, NY, 1996).
 - [26] R. Fletcher, J. C. Maan, K. Ploog, and G. Weimann, Phys. Rev. B **33**, 7122 (1986).
 - [27] S. K. Lyo, Phys. Rev. B **40**, 6458 (1989).
 - [28] C.-X. Liu, X.-L. Qi, H. Zhang, X. Dai, Z. Fang, and S.-C. Zhang, Phys. Rev. B **82**, 045122 (2010).
 - [29] W. Pan, J. S. Xia, H. L. Stormer, D. C. Tsui, C. Vicente, E. D. Adams, N. S. Sullivan, L. N. Pfeiffer, K. W. Baldwin, and K. W. West, Phys. Rev. B **77**, 075307 (2008).
 - [30] F. D. M. Haldane, Phys. Rev. Lett. **51**, 605 (1983).
 - [31] K. I. Bolotin, F. Ghahari, M. D. Shulman, H. L. Stormer, and P. Kim, Nature **462**, 08582 (2009).
 - [32] X. Du, I. Skachko, F. Duerr, A. Luican, and E. Y. Andrei, Nature **462**, 08522 (2009).